VORTICITY STRUCTURES NEAR THE TURBULENT/NONTURBULENT INTERFACE IN A PLANAR TURBULENT JET

Ricardo J. N. dos Reis
Mechanical Engineering Department
Instituto Superior Técnico
Av. Rovisco Pais, 1049-001 Lisboa
Portugal
rreis@aero.ist.utl.pt

Carlos B. da Silva
Mechanical Engineering Department
Instituto Superior Técnico
Av. Rovisco Pais, 1049-001 Lisboa
Portugal
carlos.silva@ist.utl.pt

José C. F. Pereira
Mechanical Engineering Department
Instituto Superior Técnico
Av. Rovisco Pais, 1049-001 Lisboa
Portugal
jcfpereira@ist.utl.pt

ABSTRACT

The intense vorticity and the large vorticity structures are studied using a DNS of a turbulent planar jet. The structures are characterised in the jet regarding their radius, vorticity, tangential velocity, circulation and orientation in respect to the turbulent/nonturbulent interface. The variation of their characteristics with the distance to the Turbulent/Non-turbulent interface is also documented and their effect on this interface is described. A model is presented to explain the behaviour of the enstrophy viscous diffusion term at the Turbulent/Nonturbulent interface.

INTRODUCTION

Turbulent entrainment *i.e.* the transfer of mass, momentum and passive scalars from an irrotational to a turbulent medium, is crucial to the understanding of many natural and engineering flows. The dynamics and underlying mechanisms of turbulent entrainment take place at the Turbulent/Nonturbulent interface (T/NT), defined as the separating surface between the irrotational and turbulent regions in free shear flows Corrsin & Kistler (1955).

According to the classical view on the turbulent entrainment mechanism (Townsend (1966)) "engulfing" motions induced by the large scale vortices transport "islands" of irrotational fluid into the turbulent region. This is followed by viscous enstrophy diffusion at the borders of these "islands" completing the process by which regions of irrotational fluid became turbulent. Recent experimental and numerical studies Westerweel *et al.* (2005, 2009); Mathew & Basu (2002) have shed a different light on the subject however, re-establishing the hypotheses first formulated by Corssin in the 50s (Corrsin & Kistler (1955)), *i.e.* small scale ("nibbling") eddy motions acting at the T/NT interface are the predominant mechanism

driving the entrainment by promoting a continuos diffusion of enstrophy from the turbulent into the irrotational flow region.

Albeit "nibbling" now seems to be the best explanation for turbulent entrainment several questions remain unanswered about the behavior of the T/NT interface and the scales associated with it. The work herein purports to help answer some of those through the study of the characteristics and dynamics of the intensed vorticity structures (IVS) and large vorticity structures (LVS) near this interface. For this purpose a direct numerical simulations (DNS) of a turbulent plane jet da Silva & Pereira (2008) was used. The IVS were detected with a similar vortex tracking algorithm described in Jiménez & Wray (1998). Statistics conditioned with the distance to the T/NT interface, as described in references Westerweel *et al.* (2005); da Silva & Pereira (2008), were used to assess their characteristics dependence with the distance from the T/NT interface.

The results here presented highlight the impact of the T/NT interface on these structures and vice-versa. They document the characteristics of these structures in a turbulent plane jet, showing where they depart from those present in homogeneous isotropic turbulence (HIT), namely near the T/NT interface. This study confirms the adequacy of the Burgers vortex model to describe the IVS (implying an equilibrium between the axial stretching rate and the radial viscous diffusion) inside the jet and to a smaller extent near the T/NT interface where this model is less accurate.

NUMERICAL METHODS

The turbulent plane jet DNS temporal simulation (henceforth referred has PJET) was generated using a pseudo-spectral scheme for spatial discretisation and a 3rd order, 3 step, Runge-Kutta temporal advancing scheme. Detailed de-

Table 1. Comparison of the values of several variables from the validating HIT simulation and the PJET simulation with the variation interval built from values reported in the literature (References): R radius, u_0 tangential velocity, Re_Γ circulation Reynolds number, ω_0 axial vorticity.

	HIT	PJET	References
$<R>/\eta$	4.6	4.6	4.2-5.0
$<u_0>/u'$	0.68	0.76	0.50 - 1.21
$<Re_\Gamma>/Re_\lambda^{1/2}$	28.8	28.3	10.5 - 32.4
$<\omega_0>/(\omega' Re_\lambda^{1/2})$	0.39	0.38	0.30 - 0.40

scription of it is given in da Silva & Pereira (2008).

The simulation has, in each Cartesian direction - streamwise (x), normal (y), spanwise (z) - $N_x = 256, N_y = 384, N_z = 256$, collocation points. The computational extent in each direction is $L_x = 4H, L_y = 6H, L_z = 4H$, H being the initial jet slot width. Extensive validation tests of this simulation are described in da Silva & Pereira (2008). The self-similar regime - signaled by the collapse of the second order moments - happens at $T/T_{ref} \approx 20$, time at which the jet half-width is $\delta_{0.5}/H = 0.78$. The Taylor based Reynolds number is $Re_\lambda = u'\lambda/\nu \approx 120$, with $\lambda^2 = <u'^2> / <(\partial u/\partial x)^2>$, $u' = <u'2>^{1/2}$ and ν the viscosity.

Coeherent structures detection

The intense vorticity structures (IVS) are vortical structures formed by the points of strongest vorticity, *i.e.* the 1% of points present in the flow with the highest vorticity (Jiménez *et al.* (1993)). These regions of concentrated vorticity assume either tubular or sheet like shapes. In the former, vorticity and strain exhibit similar orders of magnitude, while in the latter vorticity dominates over strain. Sheet type structures also have smaller lifetimes than vortex tubes, making the later more likely to influence the T/NT interface dynamics. To avail their behaviour, characteristics and role near the T/NT interface, the vorticity based IVS tracking algorithm described in Jiménez *et al.* (1993); Jiménez & Wray (1998) was implemented.

Verification was carried using a HIT DNS simulation with 256^3 points, $Re_\lambda = 111$ and maximum resolved wavenumber $k_{max}\eta = 1.51$ and results checked against those found in various previous studies: Jiménez *et al.* (1993); Jiménez & Wray (1998); Kida & Miura (1998); Tanahashi *et al.* (2001); Mouri *et al.* (2007); Kang *et al.* (2008). Table 1 shows that the results thus obtained for the full turbulent flow are well within the values obtained in previous studies. Comparisons with the pdfs of $<R>$, $<Re_\Gamma>/Re_\lambda^{1/2}$ and $<u_0>/u'$ against those presented in Jiménez *et al.* (1993); Jiménez & Wray (1998) were also carried with good agreement (see da Silva *et al.* (2010)).
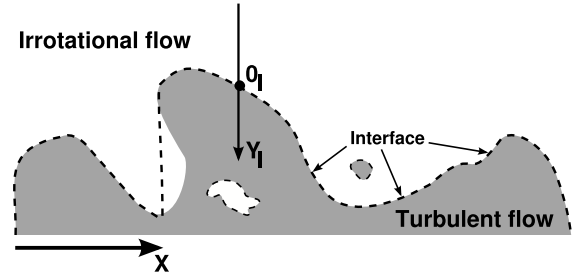
Figure 1. Sketch of the Turbulent/Non-turbulent interface showing the reference axis and islands of irrotational and of turbulent fluid.

Turbulent/Non-turbulent Interface detection

To detect the T/NT interface the same vorticity criterion methodology present in *e.g.* Bisset *et al.* (2002); Mathew & Basu (2002); da Silva & Pereira (2008); da Silva (2009) was used. The threshold value of $|\omega| = 0.7U_1/H$ is used to define the limits of irrotational/vorticity regions and thus define the location of the T/NT interface position. The conditional statistics were then obtained with the same methodology as in da Silva & Reis (2011): a local reference axis is defined with the axis centre ($y_I = 0$) located exactly at the T/NT interface position, while the irrotational and turbulent regions correspond to $y_I < 0$ and $y_I > 0$, respectively (fig 1). Statistics are then conditioned on the interface distance measured in the local axis (fig 1). Proper care was taken to eliminate irrotational or vorticity "islands" found in the rotational/irrotational regions, respectively.

RESULTS AND DISCUSSION
Turbulent/Non-turbulent Interface

A first look of the interplay between the intense vorticity structures (IVS), large vorticity structures (LVS) and the T/NT interface can be made through fig. 2 where the IVS (yellow) are portrayed with their real radius for comparison with the interface (translucent orange). A cut was made to better see the connection between the interface, IVS and the LVS, identified through pressure iso-surfaces. The T/NT interface is defined mostly by the LVS while the IVS seem to lay further below.

Intense Vorticity Structures topology near the interface

The intimate relation between the interface shape and the presence of the coherent structures, especially the LSV, emerges by observation of Fig. 2. da Silva & Reis (2011); da Silva & Taveira (2010) have shown that the LSV radius is $R_{LSV} \approx 20\lambda$, exactly equal to the thickness of the vorticity jump in the T/NT interface (fig. 3 a)). da Silva & Taveira (2010); da Silva & Reis (2011) have explained the apparent discrepancy between differing reported length scales for this thickness among several authors: of the order of η in simulations generated from an oscillating grid against λ order values for experimental round jets and DNS of plane jets has presented here. LSV are connected with the presence of mean shear in the flow. In its absence the larger coherent structures are the IVS. These have a mean radius of the order of the Kol-
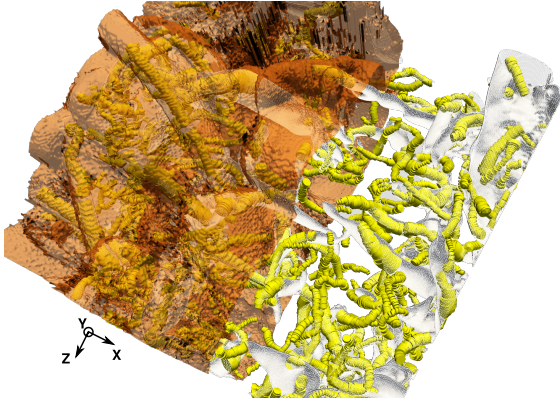
Figure 2. Turbulent/Non-turbulent interface (orange), Intense Vorticity Structures (yellow) and Large Vorticity Structures (LVS, white mesh)

mogorov micro-scale (see tab. 1). These facts support the idea that the T/NT interface is defined by the border of the largest coherent structures since their radius, in each type of flow, is very close to that reported has the T/NT interface thickness.
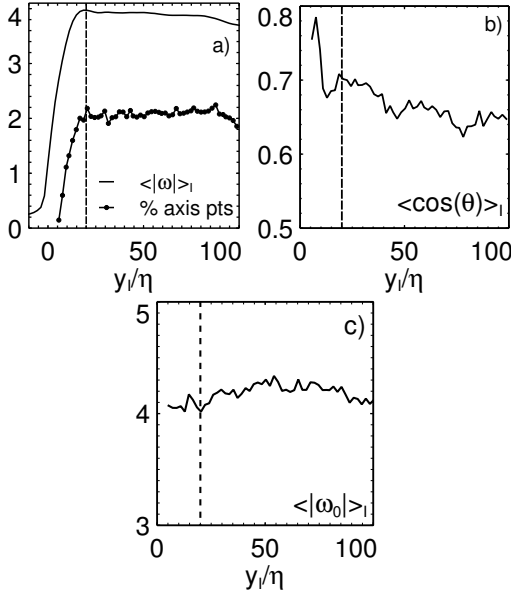
Figure 3. Statistics conditioned on the distance from the T/NT interface: a) $|\omega|$ and relative distribution of IVS in the flow (against total IVS), b) alignement of the IVS with the interface, indicated by $cos(\theta) = \omega_0 \cdot \mathbf{n}_I/(|\omega_0||\mathbf{n}_I|)$ where ω_0 is the IVS axial vorticity vector and $\mathbf{n}_I$ the interface tangent, c) axial vorticity profile. Dash vertical line at $y_I = 20\eta = \lambda$.

The number of detected IVS is relatively constant inside the jet, diminishing when approaching the interface and virtually disappearing at a distance of $\approx 5\eta$ from it (fig. 3a)). Computing the alignment between the axial vorticity of the IVS structures and the interface tangent (see fig. 3 b)), it can be seen that their alignment increases with the proximity to the T/NT interface. The axial vorticity, on the other hand, remains relatively constant throughout the whole shear layer cross-section (fig. 3 c). This indicates that the influence of the T/NT interface upon the IVS is reflected more their spatial orientation than on the magnitude of their vorticity.

Burgers vortex model

The steady Burgers vortex is an exact solution of the Navier-Stokes equations describing a vortex tube immersed in an axisymmetric, irrotational field, with a constant radius R_B due to the balance between the axial stretching rate and the radial viscous diffusion (Davidson (2004)). Vorticity and velocity (in cylindrical coordinates) are expressed by

$$\omega_z(r) = \frac{\alpha\Gamma}{4\pi\nu}e^{-r^2/R_B^2} \tag{1}$$

$$u_z = \alpha z \quad u_r = 1/2\alpha r \quad u_\theta = \Gamma/(2\pi r)\left(1 - e^{-r^2/R_B^2}\right) \tag{2}$$

where $\Gamma = 2\pi\int_0^\infty \omega_z(r)rdr$ is the vortex circulation, α the rate-of-strain and the Burgers radius expressed by

$$R_B = 2(\nu/\alpha)^{1/2}, \tag{3}$$

$\alpha = \sigma_0 = \omega_0^T \cdot \mathbf{S} \cdot \omega_0/|\omega_0|^2$, where $\mathbf{S}$ is the local rate-of-strain and σ_0 the axial stretching rate, acting in the IVS axis with axial vorticity ω_0.

Jiménez *et al.* (1993); Jiménez & Wray (1998) have shown that the Burgers vortex is a good model to describe the IVS present in HIT. In both simulations used in this work a good fitting was also found between the Burgers vortex model and the IVS: $< R/R_B >= 0.99$ in HIT and $< R/R_B >= 0.97$ for PJET (the values obtained in the literature for $< R/R_B >$ for forced isotropic turbulence are $0.95 \leq \langle R/R_B \rangle \leq 1.01$ at similar Reynolds numbers). Near the T/NT interface, however, the picture is slightly different and the Burgers model shows to be less accurate to describe the IVS: for the IVS located at $5 < y_I/\eta < 20$, $< R/R_B > \approx 0.90$ (see fig. 4 a)).

This deviation is explained by the changes in stretching rate σ_0 near the interface: although roughly constant inside the shear layer it decreases rapidly near the interface, showing a minimum at $y_I/\eta = 20$. This location is coincident with the maximum values of radius, tangential velocity and circulation of the IVS (fig. 4 b,c and d). Since the σ_0 imposed on the IVS originates from the background vorticity at the LSV edges (see Jiménez *et al.* (1993); Jiménez & Wray (1998)), and the LSV number decreases near the interface, so does σ_0. Has a result, the IVS near the interface are not in equilibrium, departing from the steady Burgers model, and their mean radius tends to increase in time. More details can be found in da Silva *et al.* (2010).

Turbulent entrainment: the nature of 'nibbling'

The enstrophy viscous diffusion term of the enstrophy transport equation is usually negligible in most turbulent
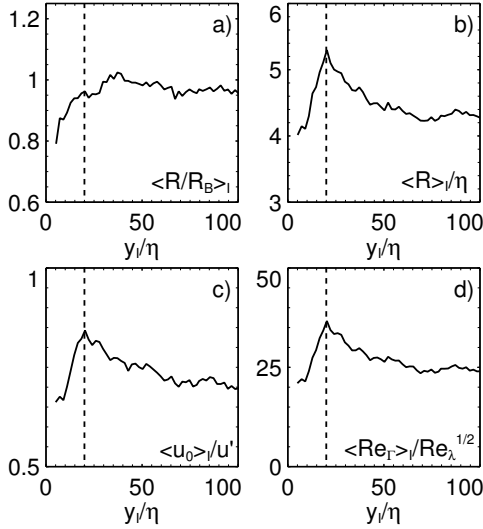
Figure 4. Mean profiles of the IVS characteristics conditioned on the distance from the T/NT interface y_I ($y_I < 0$ - irrotational region; $y_I > 0$ turbulent region) a) Radius vs. Burgers radius ($< R/R_B >_I$); b) radius ($< R >_I / \eta$); c) Axial velocity ($< u_0 > /u'$); d) Circulation based Reynolds number ($< Re_\Gamma >_I /Re_\lambda^{1/2}$). The vertical dashed line defines the point $y_I = 20\eta \approx \lambda$.

flows. Near the T/NT interface, however, it assumes a singular shape, documented by da Silva & Pereira (2007); Holzner *et al.* (2007, 2008); da Silva & Reis (2011), with a negative "dent" at $y_I \approx 10\eta$ and a peak exactly at $y_I = 0$ (see fig. 5a)). Although Holzner *et al.* (2008) has done a detailed analysis of this behaviour, correlating strain and enstrophy, an alternative, simpler explanation can be provided building upon the idea of the interface being defined by the LSV.

The LSV vorticity profile is well approximated by a Gaussian function

$$\omega(r)/\omega_0 = e^{-r^2/R^2} \qquad (4)$$

From eq. 4 the enstrophy radial profile becomes

$$\omega(r)^2/\omega_0^2 = e^{-2r^2/R^2} \qquad (5)$$

and, consequently the radial profile of the enstrophy diffusion becomes

$$\frac{\partial^2}{\partial r^2}\left[\frac{1}{2}\omega(r)^2\right] = \frac{-4\omega_0^2}{R^2}e^{-2r^2/R^2}\left(1 - \frac{4r^2}{R^2}\right). \qquad (6)$$

Equations 5 and 6 are plotted in fig. 5 b). Has can be seen the viscous-enstrophy diffusion has the same shape observed in fig. 5 a), *i.e.*, negative values inside the vortex and positive outside. This is, off course, explained by diffusive term mechanics, transporting the quantity from the highest value zone (negative inside the vortex) to the lowest region (outside), as described by Holzner *et al.* (2008). Fig. 5 c) shows a
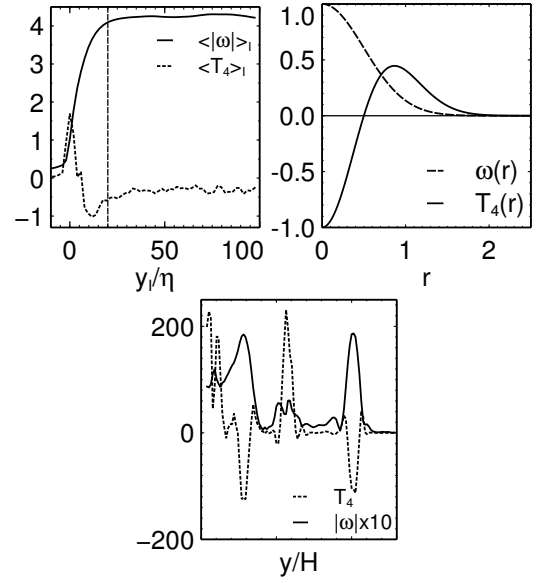
Figure 5. Mean profiles of the IVS characteristics conditioned on the distance from the T/NT interface y_I ($y_I < 0$ - irrotational region; $y_I > 0$ turbulent region) a) Enstrophy viscous diffusion $T_4 = \nu(\partial^2/\partial x_j \partial x_j)(1/2\omega_i\omega_i)$ and vorticity norm $|\omega|$. b) Profiles for the model of LSV enstrophy expressed by eq. 5 and also for the enstrophy viscous diffusion (T_4), from eq. 6. c) Instantaneous profile vorticity norm (scaled $\times10$) and enstrophy viscous diffusion near the T/NT interface between to LSV. Vertical dashed line at $y_I = 20\eta \approx \lambda$.

representative instantaneous profile of vorticity norm and enstrophy viscous diffusion near the T/NT interface. As can be seen by the two peaks in vorticity, the profile crosses two large vortices. Likewise, the aforementioned enstrophy viscous diffusion shows the same behaviour predicted by eqs 5 and 6. The differing behaviour of the enstrophy diffusion term near the T/NT interface is then explained by the LSV presence near it. More results can be found in da Silva & Reis (2011).

ONGOING WORK

Further research on the topic will be developed using a spatial jet DNS simulation in train of validation at the moment of writing. The simulation has dimensions of $L_x = 64.8H, L_y = 47H, L_z = 5.1H$ (H being the jet inlet slot width), using ≈ 1 billion collocation points. The DNS code is a parallel (MPI/Open MP), spatial pseudospectral in Y, Z directions and compact, 6th order finite-difference in the streamwise direction. Time discretisation is done with a Runge Kutta, 3rd order scheme. Visualisations of $|\omega|$ are shown in figs. 6 and 7.

Besides re-applying the same methodology expressed previously, research on the topic will be further expanded through space and temporal tracking of the coherent structures. Conditional statistics will also be pursued to further enlighten the dynamics of the "nibbling" process in turbulent entrainment.
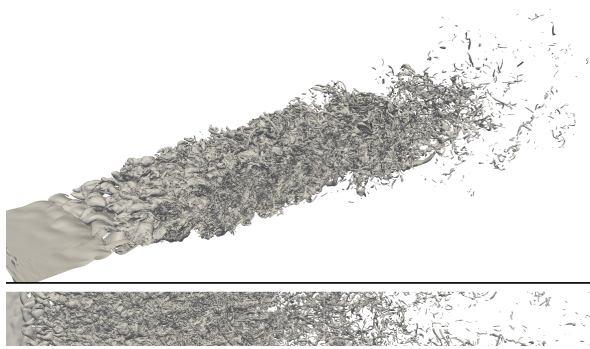
Figure 6. Perspective and top views of current vorticity norm iso-surfaces of the spatial DNS
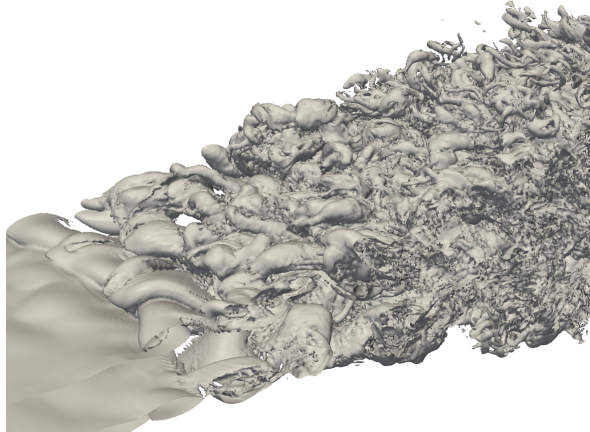
Figure 7. Detail of the transition region in fig. 6.

CONCLUSION

A detailed analysis and characterisation of the intense vorticity structures (IVS) and of the large scale vorticity structures (LVS) in a plane jet, using a temporal DNS simulation was carried out. The IVS radius was found to be similar to that found in homogeneous isotropic turbulence (HIT) and other simulations, with $R/\eta = 4.6$.

It was found that, like in HIT, the steady Burgers vortex model provides an overall good description of the IVS in the plane turbulent Jet. Differences were nevertheless found near the T/NT interface, namely a deviation from the Burgers vortex model for describing the IVS in that location. The cause is linked with a decrease of the levels of local axial stretching observed near the T/NT interface due to a decrease in the number of neighbouring LVS near the jet edge and the consequent absence of "part" of the background turbulence causing this stretching, as compared to HIT.

The particular behaviour of the enstrophy viscous term near the T/NT interface was inked to the presence of LSV near the T/NT interface, which suggests that "nibbling" is caused by the diffusion of enstrophy near the LVS at the edge of the jet.

REFERENCES

Bisset, D. K., Hunt, J. C. R. & Rogers, M. M. 2002 The turbulent/non-turbulent interface bounding a far wake. *J. Fluid Mech.* **451**, 383–410.

Corrsin, S. & Kistler, A. L. 1955 Free-stream boundaries of turbulent flows. Technical Report TN-1244. NACA.

Davidson, P. A. 2004 *Turbulence, an introduction for scientists and engineers*. Oxford University Press.

Holzner, M., Liberzon, A., Luthi, B., Nikitin, N., Kinzelbach, W. & Tsinober, A. 2008 A lagrangian investigation of the small-scale features of turbulent entrainment through particle tracking and direct numerical simulation. *J. Fluid Mech.* **598**, 465–475.

Holzner, M., Liberzon, A., Nikitin, N., Kinzelbach, W. & Tsinober, A. 2007 Small-scale aspects of flows in proximity of the turbulent/nonturbulent interface. *Phys. Fluids* **19**, 071702.

Jiménez, J. & Wray, A. 1998 On the characteristics of vortex filaments in isotropic turbulence. *J. Fluid Mech.* **373**, 255–285.

Jiménez, J., Wray, A., Saffman, P. & Rogallo, R. 1993 The structure of intense vorticity in isotropic turbulence. *J. Fluid Mech.* **255**, 65–90.

Kang, S.-J., Tanahashi, M. & Miyauchi, T. 2008 Dynamics of fine scale eddy clusters in turbulent channel flows. *Journal of Turbulence* **8(52)**, 1–19.

Kida, S. & Miura, H. 1998 Identification and Analysis of Vortical Structures. *Eur. J. Mech. B/Fluids* **17** (4), 471–489.

Mathew, J. & Basu, A. 2002 Some characteristics of entrainment at a cylindrical turbulent boundary. *Phys. Fluids* **14(7)**, 2065–2072.

Mouri, H., Houri, A. & Kawashima, Y. 2007 Laboratory experiments for intense vortical structures in turbulence velocity fields. *Phys. Fluids* **19**, 055101.

da Silva, C.B. & Reis, Ricardo J.N. 2011 The role of coeherent vortices near the turbulent/nonturbulent interface in a planar jet. *Phil. Trans. Roy. Soc. A* **369**, 738–753.

da Silva, C.B., Reis, Ricardo J.N. & Pereira, José C.F. 2010 The intense vorticity structures near the turbulent/nonturbulent interface in a jet. *J. Fluid Mech. (submitted)* .

da Silva, C. B. 2009 The behavior of subgrid-scale models near the turbulent/nonturbulent interface in jets. *Phys. Fluids* **21**, 081702.

da Silva, C. B. & Pereira, J. C. F. 2007 Enstrophy, strain and scalar gradient dynamics across the turbulent-nonturbulent interface in jets. In *Advances in Turbulence XI - 11th Euromech ETC, Porto*.

da Silva, C. B. & Pereira, J. C. F. 2008 Invariants of the velocity-gradient, rate-of-strain, and rate-of-rotation tensors across the turbulent/nonturbulent interface in jets. *Phys. Fluids* **20**, 055101.

da Silva, Carlos B. & Taveira, Rodrigo R. 2010 The thickness

of the turbulent/nonturbulent interface is equal to the radius of the large vorticity structures near the edge of the shear layer. *Physics of Fluids* **22** (12), 121702.

Tanahashi, M., Iwase, S. & Miyauchi, T. 2001 Appearance and alignment with strain rate of coherent fine scale eddies in turbulent mixing layer. *Journal of Turbulence* **2(6)**, 1–17.

Townsend, A. A. 1966 The mechanism of entrainment in free turbulent flows. *J. Fluid Mech.* **26**, 689–715.

Westerweel, J., Fukushima, C., Pedersen, J. M. & Hunt, J. C. R. 2005 Mechanics of the turbulent-nonturbulent interface of a jet. *Phys. Review Lett.* **95**, 174501.

Westerweel, J., Fukushima, C.and Pedersen, J.M. & Hunt, J.C.R. 2009 Momentum and scalar transport at the turbulent/nonturbulent interface of a jet. *J. Fluid Mech.* **631**, 199–230.